Master Thesis

Development of a 3D printed hydraulic piston-cylinder system

Ion Martinez de Apellaniz Goenaga 4754638

ME-51032
Master Thesis

TU Delft Delft University of Technology

Faculty of 3ME

October 14, 2019

Development of a 3D printed hydraulic piston-cylinder system

by

Ion Martinez de Apellaniz Goenaga

4754638

in partial fulfillment of the requirements for the degree of

Master of Science

Mechanical Engineering

Track: Biomechanical Design

Specialization: Biorobotics

to be defended publicly on Monday 14th October, 2019 at 10:00 AM

Project duration: April 2019 — October 2019

Supervisors: Prof.dr.ir. Paul Breedveld (TU Delft)
Dr.ir. Dick Plettenburg (TU Delft)
Dr.ir. Gerwin Smit (TU Delft)

An online version of this thesis is available at http://repository.tudelft.nl

TU Delft Delft University of Technology

Acknowledgements

This work is not just the Master Thesis Report that fulfils the requirement for the course ME-51032, but it also means the end of a significant period of my life: the Master at TU Delft. It has been an intense period of acquiring knowledge in different topics that I had more and less experience, while having the opportunity to meet all kind of people, from professors and staff members that guided me helpfully until students that shared similar experiences. I would like to thank Gerwin Smit for the weekly supervision, as well as Paul Breedveld and Dick Plettenburg for being part of the Committee. Costanza Culmone and Juan Cuellar also gave me useful and valuable feedback that helped with the final tweaks of presentation and report. I would also like to mention Jan van Frankenhuyzen. It has been a pleasure to receive his guidance along the tedious process of having all the necessary resources available. It would have not been possible without him to take all the necessary steps to end up with the production and testing of the actuators. He was always willing to do his best when I needed something from the university, while being always happy about his job. Thank you. Finally, I would also like to thank all the people that supported me along the project, starting with my parents and brother, that were always there, my flatmates (Zamoranus, Peibol, Nachete, Mololo and Rubenio), that accompanied me through this last year making it more enjoyable, and my friends back home, the LPM, who also helped from the distance and during the visits.

Abstract

Introduction: Recently 3D printing has received an increasing attention on the area of actuators. It can provide design freedom allowing complex geometries, as well as customization, among other benefits. However, there is no research on 3D printing of hydraulic piston-cylinder systems. The aim of this article is to check the feasibility of 3D printing a hydraulic piston-cylinder system, as well as quantifying its performance.

Methods: The same design was utilized for different 3D printing processes (Fused Deposition Modelling (FDM), Stereolithography (SLA) and Selective Laser Melting) and materials (Polylactic Acid (PLA), resin and Titanium), in order to be compared with each other and with conventional manufacturing of a system in Aluminum. Also, a second version of each piston-cylinder system was printed to use a reamer on them, to compare the performance between the cylinders with and without reaming. The followed methodology consisted of performing static and dynamic tests for each of the actuators. The output of the static test was the maximum fluid pressure that the system can handle. With the dynamic test a more realistic situation could be tested, from which the friction could be deducted and its results could be compared to the theoretically calculated data.

Results: The results showed that the best performing 3D printed option was the reamed SLA resin version, reaching pressures of at least 4 MPa, with a dynamic friction force of 6.6 N, a stick-slip friction force of 9.9 N and a weight of 28 g. These features led to a force-to-weight ratio of 2928, only surpassed by the lighter FDM printed PLA actuator, reaching a value of 3565, but with higher friction forces.

Conclusion: The conducted research means a first step towards the 3D printing of hydraulic piston-cylinder systems, demonstrating that it is possible to reach high pressures without leakage. The features that additive manufacturing offers, such as lighter and customized geometries in one assembly step, can benefit application fields where hydraulic piston-cylinders are used, such as prosthetic devices.

Nomenclature

$\boldsymbol{a}$	Acceleration (m/s^2)
$\boldsymbol{A}$	Area of the piston where the fluid is acting (m^2)
Al	Aluminum
$\boldsymbol{CD}$	Cross-sectional Diameter of the O-ring (mm)
$\boldsymbol{CompD}$	90% of the Cross Sectional Diameter of the O-ring (mm)
$\boldsymbol{CRing}$	Part of the Inner Diameter of the cylinder occupied by the squeezed O-ring (mm)
$\boldsymbol{F}$	Force actuating on the piston (N)
$\boldsymbol{F_{fric}}$	Frictional force (N)
$\boldsymbol{F_{stick}}$	Frictional force due to stick-slip (N)
FDM	Fused Deposition Modelling
$\boldsymbol{g}$	Gravitational acceleration (m/s^2)
$\boldsymbol{ID}$	Internal Diameter of the O-ring (mm)
$\boldsymbol{m}$	Mass (kg)
LBM	Laser Beam Melting
$\boldsymbol{OD}$	Outer Diameter of the O-ring (mm)
$\boldsymbol{P}$	Theoretical pressure of the system´s fluid (Pa)
$\boldsymbol{PGD}$	Piston Groove Diameter (mm)
PLA	Polylactic Acid
$\boldsymbol{P_{ave}}$	Average measured Pressure between the top and bottom plateaus of each weight (MPa)
$\boldsymbol{P_{peak}}$	The local maximum/minimum pressure measured in each peak (MPa)
$\boldsymbol{P_{plat}}$	Average measured Pressure of each plateau (MPa)
$\boldsymbol{P_{plats}}$	Average measured Pressure of the top plateaus of each weight (MPa)
SLA	Stereolithography
SLM	Selective Laser Melting
$\boldsymbol{Sq}$	Squeezed 10% of the Cross Sectional Diameter of the O-ring (mm)
Ti	Titanium
$\boldsymbol{\Delta\ P}$	Pressure difference between the plateaus and the average due to the friction (MPa)
$\boldsymbol{\Delta\ P_{stick}}$	Pressure difference between each plateau and its peak due to the stick-slip (MPa)

Contents

List of Figures

List of Tables

1 Introduction

1.1 3D printing

Additive manufacturing, also referred to as 3D printing, Rapid Prototyping or Solid Freeform Fabrication, is the process of making three dimensional solid objects from a digital file. After a few decades of development, there are many different 3D printing methods that are used in different production processes, or even replace the conventional production processes. Additive manufacturing, usually performed layer by layer, has been claimed to lead the third industrial revolution [5]. Even if it has not been reached yet, lot of progress is being achieved lately.

With applications in different sectors, recently an extensive list of 3D printing methods have been developed and improved: from the most affordable option that is reaching the user´s homes, printing polymers by Fused Deposition Modelling (FDM), until the printing of metal parts with a precision of micrometers via Laser Beam Melting (LBM), commonly called Selective Laser Melting (SLM) [6]. This progress is motivating further research on areas like bioprinting of complex living organs, which would allow in situ repairing of human tissue [7] or the 3D printing of soft actuators [8].

1.2 3D printed actuators

Additive manufacturing provides more design freedom allowing customized geometries, the option of assembly-free mechanisms leading to lower production times and costs, and the possibility to fast prototype [9]. Actuators are also taking advantage of these benefits over other conventional production methods. An actuator is a device responsible for generating a movement in a mechanism or system. While sensors make conversions between different forms or energy, actuators make a conversion from one form of energy to a mechanical movement [10]. Traditionally most of the actuators are activated via electricity, hydraulics or pneumatics [11], whereas recent developments have led to designs powered by photo-actuation [12] or via magnetic energy sources [13].

Additive manufacturing offers a new handful of characteristics that can drastically change the conception of an actuator. The recent demands on different applications such as robotics, biomedicine or aeronautics require certain features on certain components, including actuators, that could not be achieved the same way with other manufacturing processes. Soft actuators have become a trend for human-machine interaction allowing safe manipulation [14], micro-scale actuators are required for in-vivo human applications [15], implying biocompatibility, and light and robust actuators are demanded in the aerospace sector with fewer assembly components than before [16].

Taking a look at the number of articles published in the last few years, there is no doubt about the significance of the use of 3D printing for all kind of actuators, including different materials such as plastics, as shown in Figure 1, metals or photopolymer resins. The research within the field of additive manufacturing is of vital relevance to continue with the development of robotic and automated systems that carry out increasingly complex tasks and interact more closely with humans.

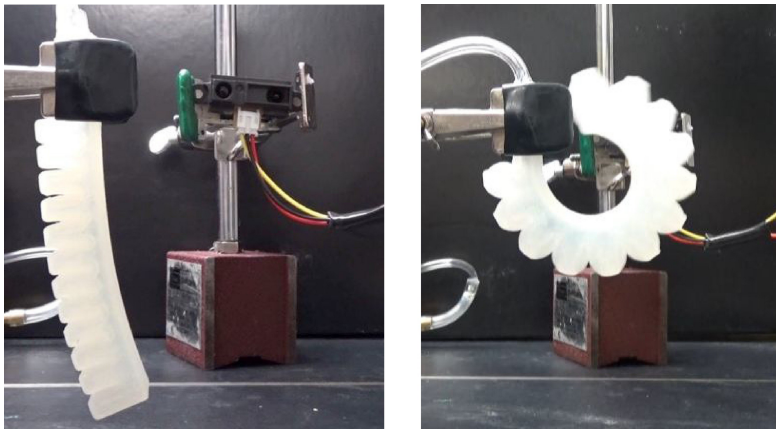

Figure 1: A 3D printed pneumatic soft polymeric actuator [1].

1.3 3D printing of piston-cylinder systems

The kinds of actuators where additive manufacturing has been used as the manufacturing process are soft actuators [17]. However, actuators that are not soft can also benefit from the advantages of 3D printing, such as the possibilities of design freedom leading to customization and lightweight structures. Figure 2 shows an FDM printed pneumatic cylinder combined with a steel piston, which can withstand pressures of up to 1 MPa [2].

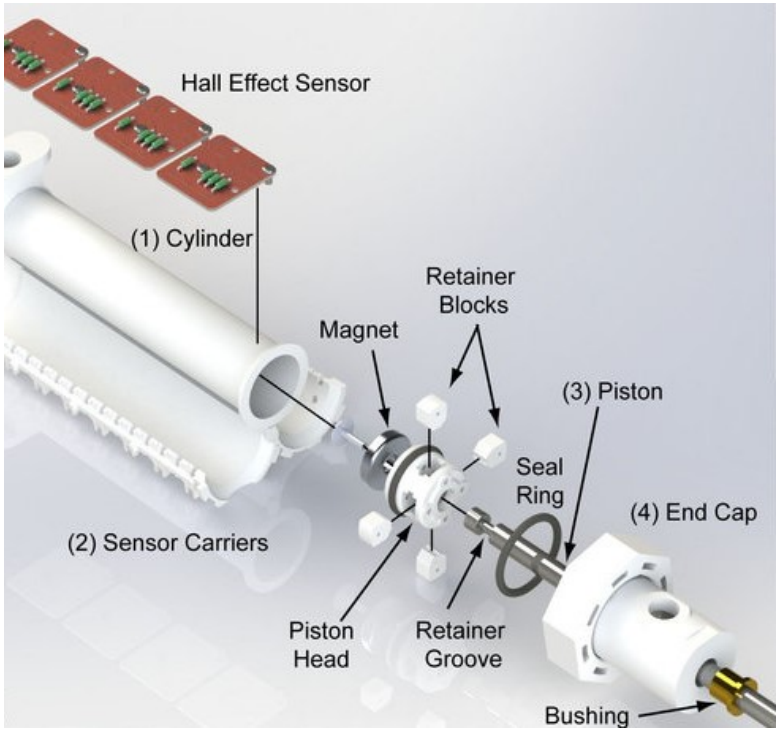

Figure 2: FDM printed pneumatic piston-cylinder system [2].

Apart from the mentioned pneumatic actuator, no other additively manufactured piston-cylinder systems have been found. Still, there are many applications where piston-cylinders are used [18], from the largest scale applications where high loads are demanded, such as construction machines, until smaller scale applications such as aviation components where the weight is more critical. Some of these applications could benefit from the advantages of 3D printing, being a prosthetic hand a clear example. Figure 3 shows the The Delft Cylinder Hand, a body-powered prosthetic hand actuated via hydraulic piston-cylinder systems [19]. The prosthesis has been almost 3D printed, except for the piston-cylinder systems. If these could also be additively manufactured, the hand could be produced in one step, sparing the assembly steps after printing. Also, it would make customization easier, as well as making the resulting prototype lighter if polymers were used, instead of the conventionally machined metals.

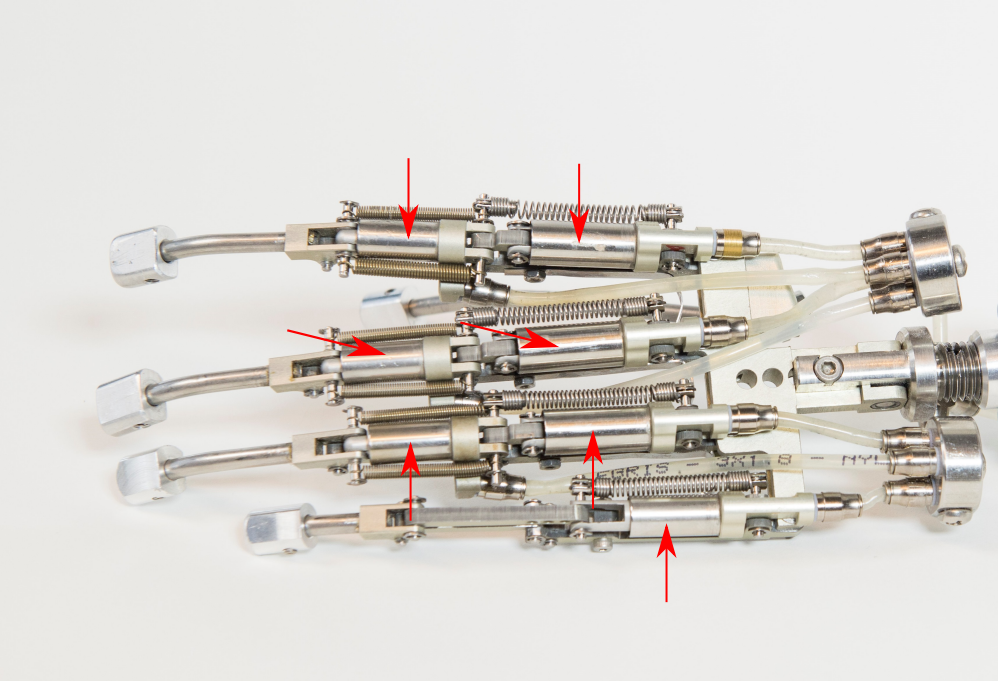

Figure 3: Delft Cylinder Hand [3]. The arrows indicate the position of the hydraulic piston-cylinder systems.

1.4 Problem definition

Given the state of the art, there is a knowledge gap about 3D printed hydraulic piston-cylinder systems. It is not known if it is possible to benefit from the advantages of additive manufacturing with 3D printed hydraulic piston-cylinder systems, neither how they would perform.

1.5 Goal

The goal of this Master Thesis is to check the feasibility of 3D printing a hydraulic piston-cylinder system, as well as quantifying its performance regarding relevant parameters. Different 3D printing processes and materials will be compared with each other and with conventional manufacturing of a hydraulic piston-cylinder system, to point out the best performing option.

2 Methodology

In this section the methods used for the development and evaluation of the 3D printed hydraulic piston-cylinder systems are explained. Firstly the design process is explained, followed by the tests performed to evaluate the designs.

2.1 Design considerations

There are mainly two types of piston-cylinder systems: single and double acting ones. The Delft Cylinder Hand works with a single acting hydraulic piston-cylinder system, meaning that the operating stroke is generated in one single direction. The return stroke can be enabled via a spring, as in the case of the Delft Cylinder Hand, or by its weight, which is the case of this article.

The main components of a piston-cylinder system are the cylinder itself, the cylinder head or end, the piston, the piston rod and the seal, as indicated in Figure 4. In this section the design of each of these parts is explained. The piston and piston rod have been developed as a single cylinder block with the grooves for the seal, for simplicity and to add strength to the part.

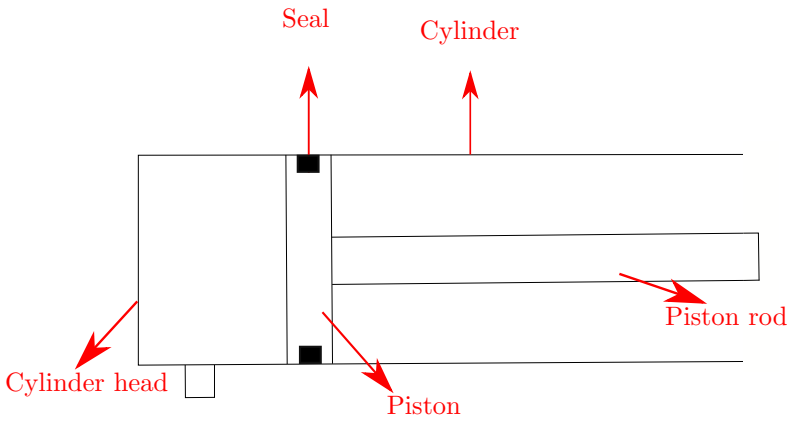

Figure 4: Main components of a piston-cylinder system.

2.1.1 Seal selection

One of the most critical components in a hydraulic piston-cylinder system is the seal [20] that makes sure the fluid is contained in the desired volume, preventing it from escaping to other areas or the outside of the system. In fact, leakage can cause loss of pressure in the chamber and contamination of the environment in the case of a harming fluid [21]. At the same time, the seal needs to minimize the friction between the cylinder and piston to avoid heat production, acceleration of wear of components and increase the efficiency of the system.

There are different kinds of seals existing in the market. For piston-cylinder systems, piston and rod seals are usually specifically designed. However, these also require other additional components such as wear rings, buffer seals, wipers and static gland seals [22]. In order to minimize the parameters of the system, O-rings were chosen as the one-component seal that would simplify installation and groove design. The O-rings, also known as packing or toric joints, are mechanical gaskets with the shape of a torus and are characterized by their low cost and easy production.

The dimension of the O-ring would determine design constraints for the rest of the components of the piston-cylinder system. The following requirements were considered:

- The resulting system needs to be printable by different processes in terms of size, considering the buildplate dimensions of each 3D printer.
- The parts of the piston-cylinders need to be adequate for the standard testing components, such as manometers, tubings or connections. If the design is too small, it will be hard to test and will need more specific tools.
- The outer diameter of the O-ring should be a whole number in mm, to allow the use of metric tools for post-processing.
- The Shore hardness of the O-ring has to ensure the durability of the seal while allowing the appropriate squeeze or rate of compression, of around 10%, as recommended by the manufacturer [23].

Checking the O-ring selector [4] the chosen O-ring was of dimensions 9x3.5 mm (Internal diameter x cross-sectional diameter), as shown in Figure 5, with a Shore hardness of 70.

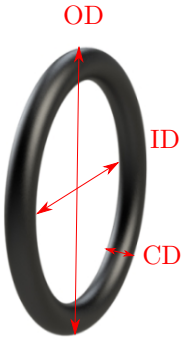

Figure 5: Eriks O-ring [4] with its characteristic lengths indicated: the Cross-sectional Diameter (CD), the Internal Diameter (ID) and the Outer Diameter (OD).

2.1.2 Parts design

The system was split into three different parts: “Piston”, “Cylinder” and “End Cap”. The End Cap and the cylinder could have been the same component, but it was differentiated into two parts to make the post-processing of the cylinder easier, being open from both sides. Afterwards, glue could be used to assemble both parts permanently. Solidworks (Solidworks Corp. Dassault Systèmes, Suresnes, France) was the modelling software used for the design of the parts.

The internal diameter (ID) of the cylinder should be equal to the external diameter (OD) of the chosen O-ring:

$$ID + CD * 2 = OD \tag{1}$$
$$9 + 3.5 * 2 = 16\ mm \tag{2}$$

where,

ID	Internal Diameter of the O-ring (mm)
CD	Cross-sectional Diameter of the O-ring (mm)
OD	Outer Diameter of the O-ring (mm)

However, the diameter of the piston groove, should not be the same as the internal diameter of the O-ring. For a squeeze of 10% on the O-ring, a larger piston groove diameter is needed:

$$10\%\ of\ CD = Sq \tag{3}$$
$$CD - Sq = CompD \tag{4}$$
$$CompD * 2 = CRing \tag{5}$$
$$OD - CompRing = PGD \tag{6}$$
$$\tag{7}$$

$$10\%\ of\ 3.5 = 0.35\ mm \tag{8}$$
$$3.5 - 0.35 = 3.15\ mm \tag{9}$$
$$3.15 * 2 = 6.3\ mm \tag{10}$$
$$16 - 6.3 = 9.7\ mm \tag{11}$$

where,

Sq	Squeezed 10% of the Cross Sectional Diameter of the O-ring (mm)
$CompD$	90% of the Cross Sectional Diameter of the O-ring (mm)
$CRing$	Part of the Inner Diameter of the cylinder occupied by the squeezed O-ring (mm)
PGD	Piston Groove Diameter (mm)

With an internal diameter of 16 mm for the cylinder and a piston groove of 9.7 mm of diameter, a squeeze of 10% is achieved (the resulting cross sectional diameter will be 2.7 mm instead of 3 mm). Figures 6, 7 and 8 show the rest of the dimensions. A wall thickness of 2 mm was chosen for the cylinder to provide enough strength while avoiding too much material. The top of the cylinder was chamfered to facilitate the insertion of the piston with the O-ring. The same chamfer was added on the End Cap to allow the insertion of the cylinder to glue. The edges on the groove of the piston were also rounded to avoid damaging the O-ring during its installation. The missing dimensions "A" and "B" will be explained later, since, depending on the production process and material, the tolerances are different.

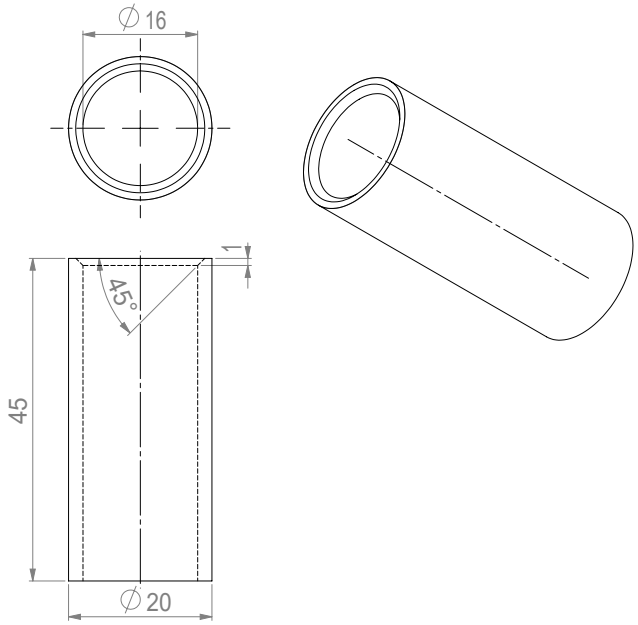

Figure 6: Drawing of the Cylinder with all its dimensions in mm.

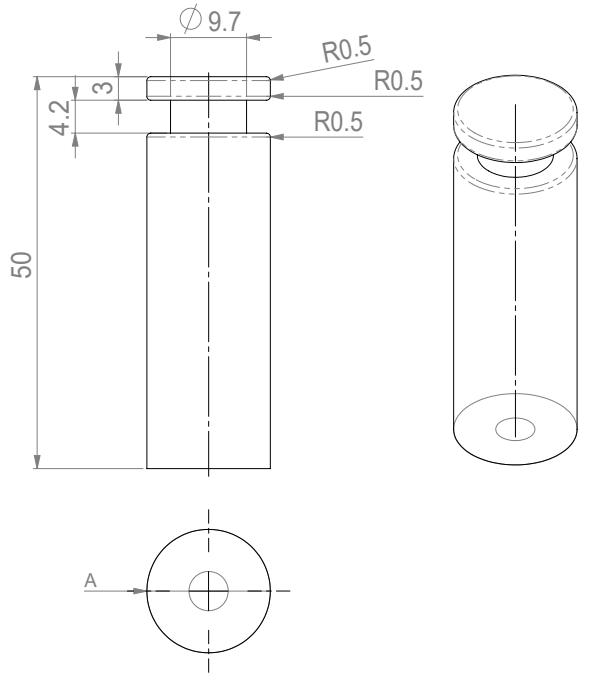

Figure 7: Drawing of the Piston with all its dimensions in mm. The external diameter "A" is a parametric dimension that will change according to the production method and material.

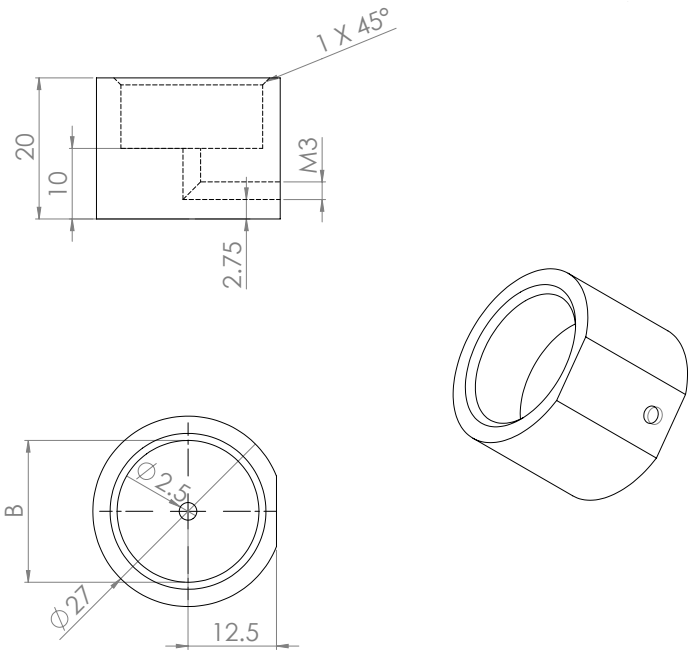

Figure 8: Drawing of the End Cap with all its dimensions in mm. The internal diameter "B" is a parametric dimension that will change according to the production method and material.

2.1.3 Production method and material selection

Three different 3D printing methods were compared to a conventionally machining of Aluminum. Each of them used a different material, with its particular dimensions according to the corresponding tolerances.

FDM in PLA

The first production method chosen for this study was FDM that is characterized by its simplicity, user-friendliness, versatility of polymers and low cost [24]. White PLA material (further information can be found in Appendix A) was selected due to its printability at high printing speeds and low melting temperature [25]. Furthermore, the piston-cylinder system was printed using the Ultimaker 3 (Ultimaker B.V. Geldermalsen, The Netherlands) due to its possibility of dual extrusion (further information can be found in Appendix B). Dual extrusion allows the use of PVA as support material, which can be then removed by immersion in water. In this way, the support removal is facilitated, ensuring a better surface finish on the supported areas. Based on trials and errors, the remaining two dimensions "A" and "B" were defined. The external diameter of the piston "A" was set to 15 mm, to allow the sliding between the piston and the cylinder with a hole of 16 mm in diameter. The internal diameter of the End Cap "B" was set to 20.4 mm for a tight fit to allow glueing.

The used slicer software used was Cura 4.0.0, from the same manufacturer of the printer. The main printing settings are shown in Figure 9. A low printing layer height (0.1 mm) was chosen for more precise printing, with high infill (50%) for the strength of the part and support to allow overhangs.

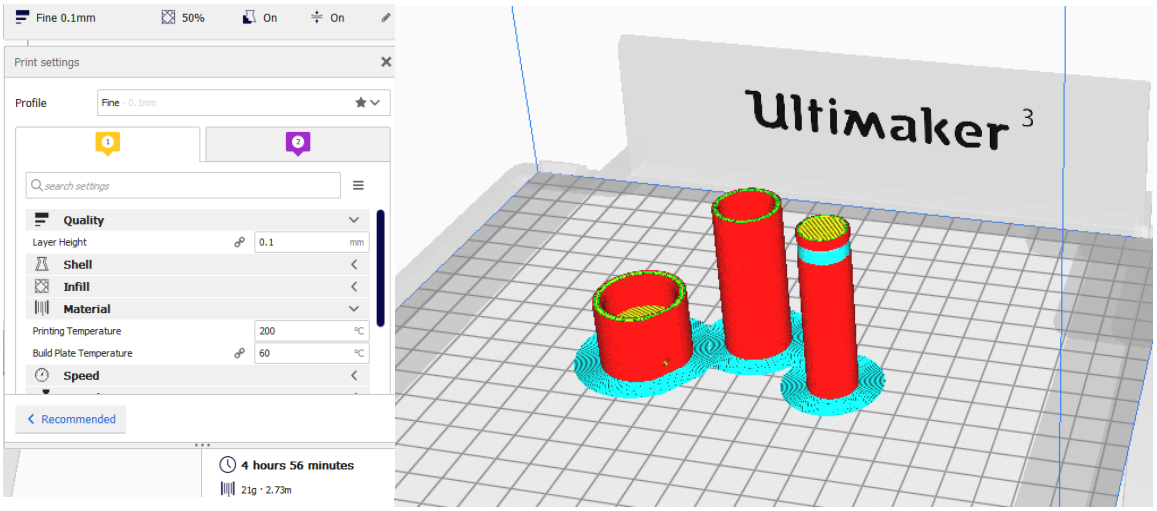

Figure 9: Cylinder, Piston and End Cap for 3D printing in the Ultimaker 3 printer, using the Cura slicer. The main settings are also visible on the left.

SLA in resin

Stereolithography (SLA) is the second selected printing process to manufacture the piston-cylinder system. The SLA is characterized by a higher dimensional accuracy with smaller printing layer heights and smoother surface finishes in different resins [26]. The piston-cylinder system was printed using the Form 2 (Formlabs. Somerville, Massachusetts, USA) printer (further information can be found in Appendix B). Among the available resins, Gray Standard Resin (further information can be found in Appendix A) was chosen because of its smooth surface finish and lower cost. The same material was used as support. Checking the tolerances of SLA printing [27], the remaining two dimensions "A" and "B" were defined. The external diameter of the piston "A" was set to 15.75 mm, to allow the sliding between the piston and the cylinder with a hole of 16 mm in diameter. The internal diameter of the End Cap "B" was set to 20.05 mm for a tight fit to allow glueing.

The used slicer software was Preform, from the same manufacturer of the printer. The orientation of the parts needs to be angled for SLA printing, to maintain a small surface area for each cross section and to avoid printing layers with large jumps in surface areas [28]. Still, the inclination could not be too high to avoid support on the critical surfaces that would provoke undesired irregularities. This is presented in Figure 10, as well as the principal printing parameters.

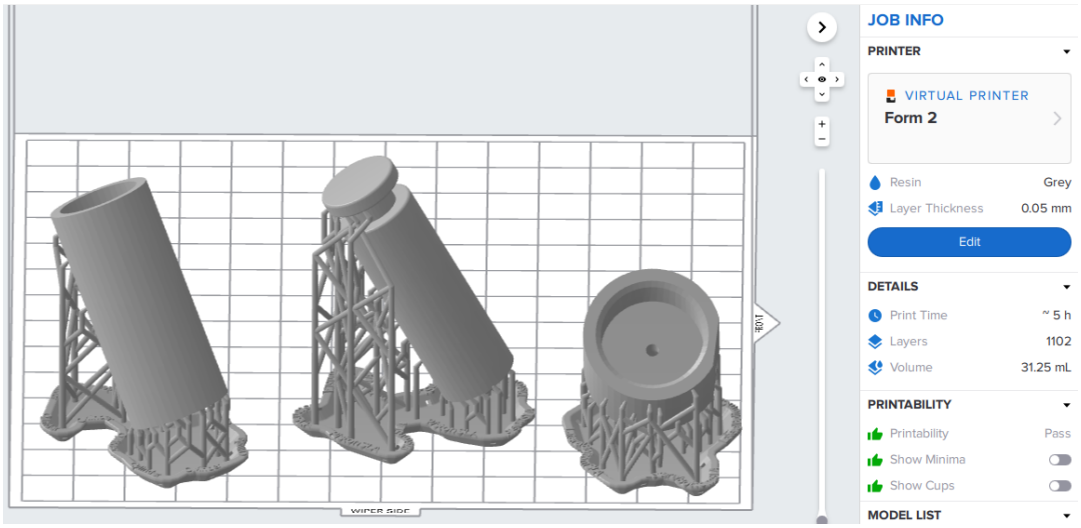

Figure 10: Cylinder, Piston and End Cap for 3D printing in the Form 2 printer, using the Preform slicer. The main settings are also visible on the right.

SLM in Titanium

The final 3D printing process analyzed was SLM, that allows printing complex designs in metal that could be much harder to manufacture via conventional methods. SLM minimizes the weight of the product while reducing the assembly time and amount of parts [29]. Titanium (Ti-6Al-4V grade 23 powder supplied by AP&C with a particle size ranging from 10 to 40 µm) was the chosen metal because of its excellent force-to-weight ratio, corrosion resistance and low thermal expansion, apart from the fact that it is biocompatible [30] (further information can be found in Appendix A). Checking the tolerances of SLM printing [31], the remaining two dimensions "A" and "B" were defined. The external diameter of the piston "A" was set to 15.5 mm, to allow the sliding between the piston and the cylinder with a hole of 16 mm in diameter. The internal diameter of the End Cap "B" was set to 20.2 mm for a tight fit to allow gluing.

The used printer was a SLM 125 machine (Realizer GmbH, Borchen, Germany) equipped with a YLM-400-AC Ytterbium fiber laser (further information can be found in Appendix B). Figure 11 shows the slicer, with the main printing parameters.

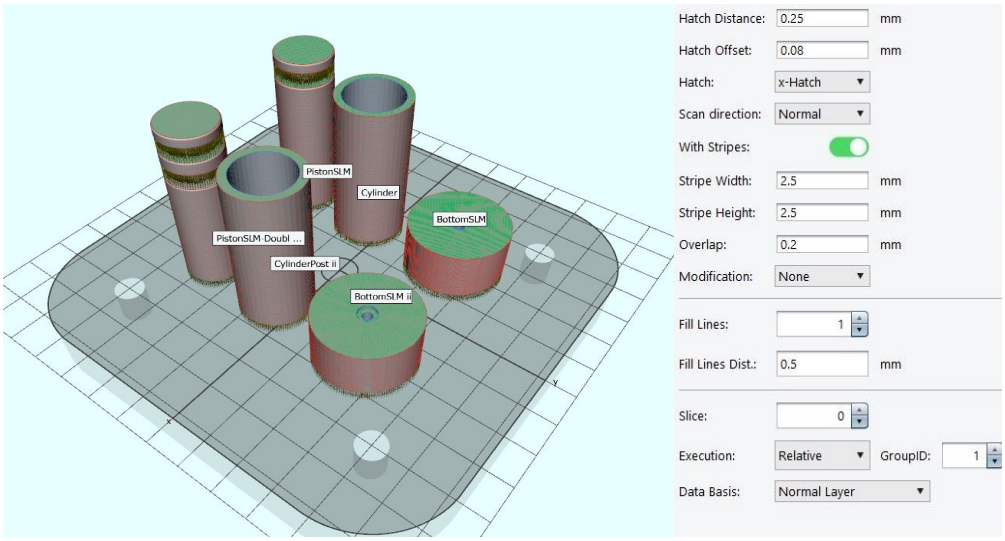

Figure 11: Cylinder, Piston and End Cap (doubled) for 3D printing in the SLM 125 printer. The main settings are also visible on the right.

Machining Aluminum

The three 3D printing methods were compared with the conventionally manufactured piston-cylinder system: machining. Aluminum (Al) was the chosen material because of its high strength-to-weight ratio, lower cost and corrosion resistance [32].

For the machining process, the drawings of the parts were needed, which were made by Solidworks as well. The tolerances were defined in the drawings, requiring higher precision for the critical dimensions, whereas the rest could have a higher range of error from the nominal value. Based on experience, the remaining two dimensions "A" and "B" were defined. The external diameter of the piston "A" was set to 15.75 mm, to allow the sliding between the piston and the cylinder with a hole of 16mm in diameter. The internal diameter of the End Cap "B" was set to 20.1 mm for a tight fit to allow gluing.

2.1.4 Post-processing steps

After printing or machining, the parts needed to be glued and threaded to allow the connection to the test set-up. Also, a second version of each piston-cylinder system was printed to use a reamer on them, to compare the performance between the cylinders with and without reaming. A reamer is a rotatory tool that makes a previously existing hole slightly larger with high precision while leaving a smooth surface [33]. A lathe was used for reaming, at low rotatory speed and with the help of lubrication. A reamer of 16 mm diameter was used to end up with a cylinder with the same inner diameter. For the cylinders that were printed to be reamed, an inner diameter of 15.8 mm was specified, to have a small layer of material to be removed by the reamer. In the case of the Titanium (Ti) cylinder, the reamer could not be used because of the strength of the Ti material. Therefore, a drill was used to try to improve the surface.

FDM in PLA

Once the parts were removed from the buildplate, they were immersed in warm water for a few hours until the PVA support was completely removed. A tap was used to create the M3 thread on the 2.5 mm hole of the End Cap, for the connection of the part to the hydraulic test set-up. The End

Cap and the cylinder were adhered by the glue "Loctite 401", which were glued at least 24 hours before the first test to allow curing.

SLA in Resin

After printing, the parts needed to be placed in an alcohol bath followed by UV curing for 20 minutes at 60 degrees. The support was removed with the help of small pliers. The same tap and glue were used again to create the M3 thread on the End Cap and to assemble the system, with the same curing time.

SLM in Titanium

The support removal was performed with pliers, followed by the use of a vacuum cleaner to get rid of the remaining loose powder. As the threading tap was not strong enough for Ti, an Al End Cap was used instead. To glue the Ti cylinder to the Al End Cap, "Araldite AV 138" glue was used, which also needed 24 hours as curing time.

Machining Aluminium

The machined parts did not need any post-processing steps apart from adding the thread plus gluing. "Loctite 401" was used once again.

2.2 Evaluation of the design

In order to compare the performance of each production method and material, the same testing procedure was used. The assembled piston-cylinder system was connected to the 4 mm inner diameter tubing via an M3 threaded connector. Via a T connector, a sensor was added to the system than can measure up to 4 MPa. A data acquisition system connected the sensor to the computer, which enabled to record the measured pressure via a Labview program. Water was used as a unique actuation fluid. For the installation of the O-ring on the piston groove, a wooden stick was used as a helper to avoid any damage on the O-ring itself or on the piston. Once an O-ring was installed, it was not removed to avoid damaging during the disassembly. In order to help the piston slide in the cylinder, a "Rocol Kilopoise 0001" lubricant was used.

2.2.1 Static test set-up and protocol

The first test consisted on measuring the maximum pressure in a static configuration before leakage appeared, the set-up broke or the maximum of the sensor was reached. Figure 12 presents the schematic test set-up in a simplified version. Figure 13 shows how this was achieved by clamping the piston-cylinder system in a press to increase the applied pressure gradually, while recording the measured pressure on the computer. The followed protocol is explained below:

- The piston-cylinder system was clamped in a press in a vertical position, so that the initial pressure was zero.
- The pressure was gradually increased by rotating the handle, at a rate of approximately 0.1 MPa per second.
- If the maximum pressure of the sensor was reached without leakage or breakdown, the experiment was finished.
- If leakage or breakdown were reached, the experiment was also finished.
- The initial stroke was set higher than 20 mm to allow enough compression of the piston-cylinder system and to be able to reach high pressures before the end of the stroke.

- The piston-cylinder system was positioned straight to ensure that the piston and cylinder were coaxial, so that lateral forces were avoided.
- When the maximum pressure was reached, the pressure was released gently.

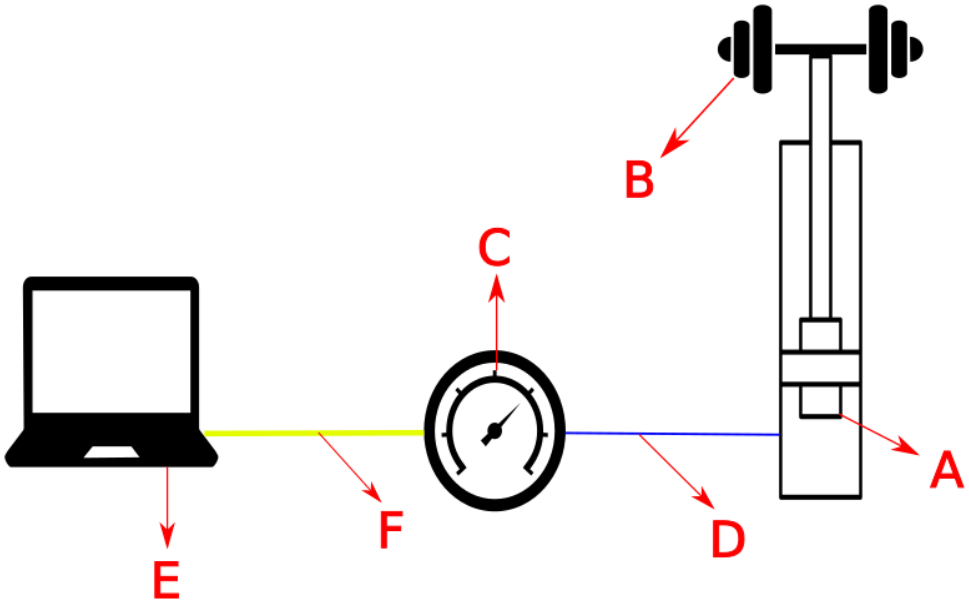

Figure 12: Schematic static test set-up: The piston-cylinder system (A) is actuated by an external force (B). The system is connected to a 4 MPa sensor (C) via hydraulic tubing (D). The sensor is connected to the laptop (E) via electrical connection (F).

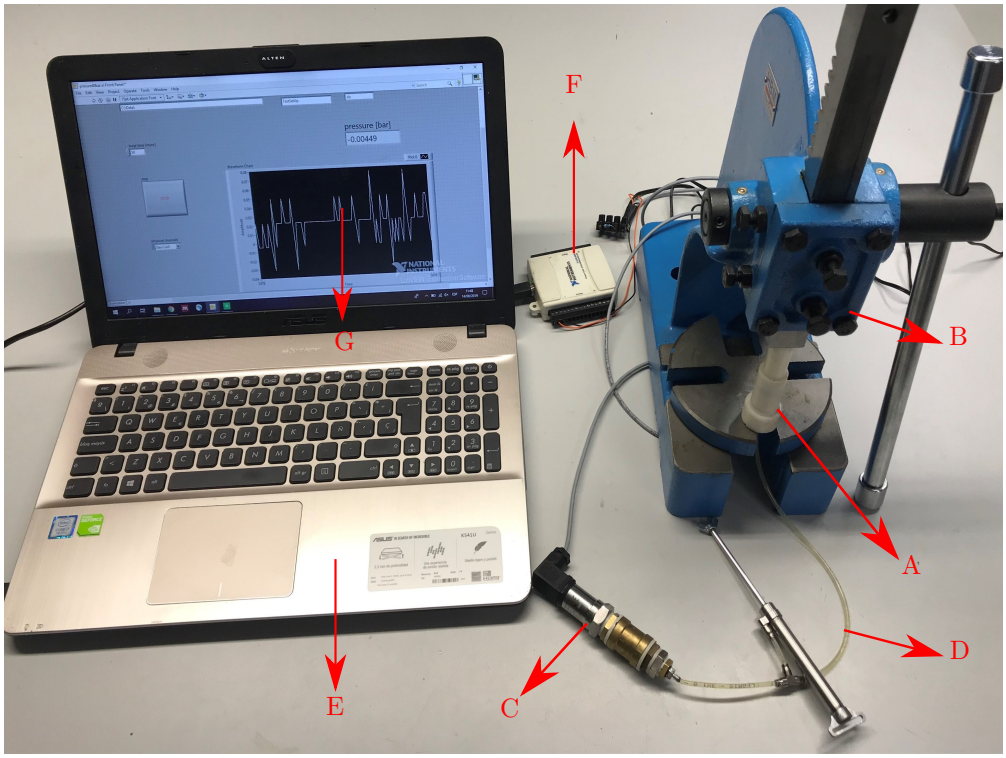

Figure 13: Real static test set-up: The piston-cylinder system (A) is placed in the press (B). The system is connected to a 4 MPa sensor (C) via a tube (D). The sensor is connected to the laptop (E) via a data acquisition system (F). The laptop displays the measured pressure with a Labview programme (G).

2.2.2 Dynamic test set-up and protocol

The second test consisted on measuring the pressure in a more realistic situation. The simplified schematic test set-up is shown in Figure 14. The objective of the piston-cylinder configuration is to provoke movement, leading to a mechanical force, induced by a pressure change on the working fluid. The way to emulate it was by placing one slave piston-cylinder system vertically clamped in a vice, helped by a 3D printed block, as indicated in Figure 15. From the 3D printed part attached to the piston, a cable hanged with a hook where weights could be placed, without touching the floor. Another piston-cylinder system was placed on the press to actuate as a master cylinder. A duplicated reamed SLA piston-cylinder was used as the master cylinder. After applying pressure to the water by compressing the master cylinder with the press, the slave piston went up, and the weights hanging from it were the ones in charge of ensuring that the piston would come back down once the pressure was released. In this way, a cyclic movement could be achieved. The followed protocol is explained below:

- Initially, the pressure in the system´s water was zero. For that, regardless of the hanging weight, the slave piston was touching the End Cap, being the initial stroke zero in the slave cylinder. On the master cylinder, a minimum initial stroke of 15 mm was needed to allow enough displacement in both cylinders during actuation.
- Later on, the weights were added progressively by 4 kg every time. From 2.25 kg, and later on to 6.25, 10.25, 14.25, 18.5 and 22.25 kg. This was done by adding weight discs to the hook.
- For each weight:

1. The master cylinder was activated until the weight was lifted, reaching a stroke of at least 10 mm in the slave cylinder
2. The press was held to maintain it there for around 8 seconds, followed by going back half of the stroke for another 8 seconds.
3. After this, the stroke was brought back to the same position of at least 10 mm stroke during another 8 seconds.
4. The master cylinder was decompressed gently until the pressure on the system´s fluid was back to zero.

- After testing each weight, it took at least 8 seconds to increase the 4 kg.

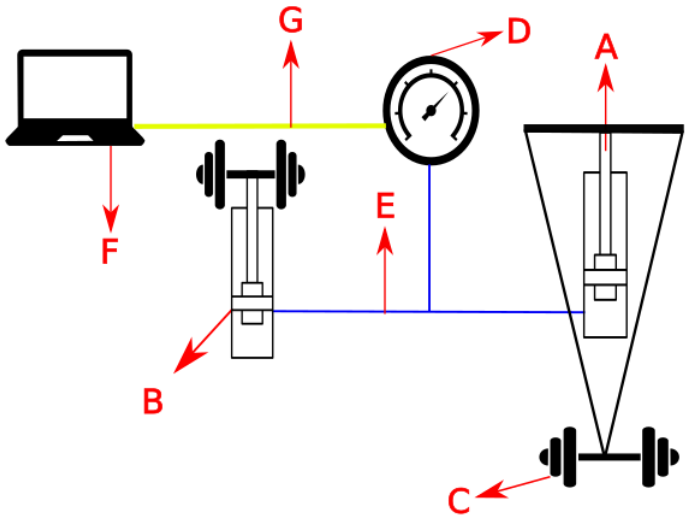

Figure 14: Dynamic test set-up: The slave piston-cylinder system (A) is actuated by the master piston-cylinder system (B). From the slave piston-cylinder system (C), a weight (C) hangs to test different masses. Both cylinders are connected to a 4 MPa sensor (D) via hydraulic tubing (E). The sensor displays the measured pressures in the laptop (F), which is connected by electronic wiring (G).

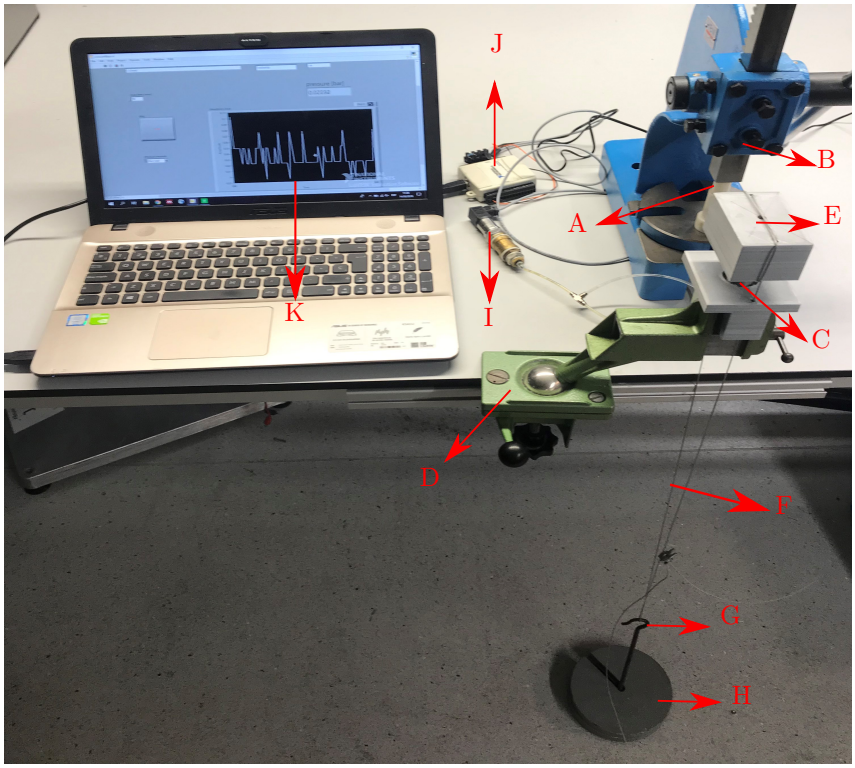

Figure 15: Dynamic test set-up: The master piston-cylinder system (A) is placed in the press (B). The slave piston-cylinder system (C) is placed in a vice (D) with the help of a 3D printed part (E). From the 3D printed part attached to the slave piston, a cable (F) hangs with a hook (G) with weight discs (H). The system is connected to a 4 MPa sensor (I) via a tube. The sensor is connected to the laptop via a data acquisition system (J). The laptop displays the measured pressure with a Labview programme (K).

3 Results

In this section the obtained results of different piston-cylinder systems are presented, as well as the outcome after the evaluation of these actuators.

3.1 Designs

For each production method the piston-cylinder systems were weighted. The weight of each component of the piston-cylinder system is indicated in Table I. The presented values for the cylinders were obtained by weighting the unreamed versions.

Table I: Weight in grams of the cylinder, piston, End cap and total for each of the production processes.

Production method	**Weights (g)**			
	Cylinder	Piston	End Cap	Total
FDM	6	9	8	23
SLA	6	11	10	28
SLM	17	27	20	64
Machined	14	26	16	56

3.1.1 FDM in PLA

Figure 16 presents the obtained FDM printed hydraulic piston-cylinder system.

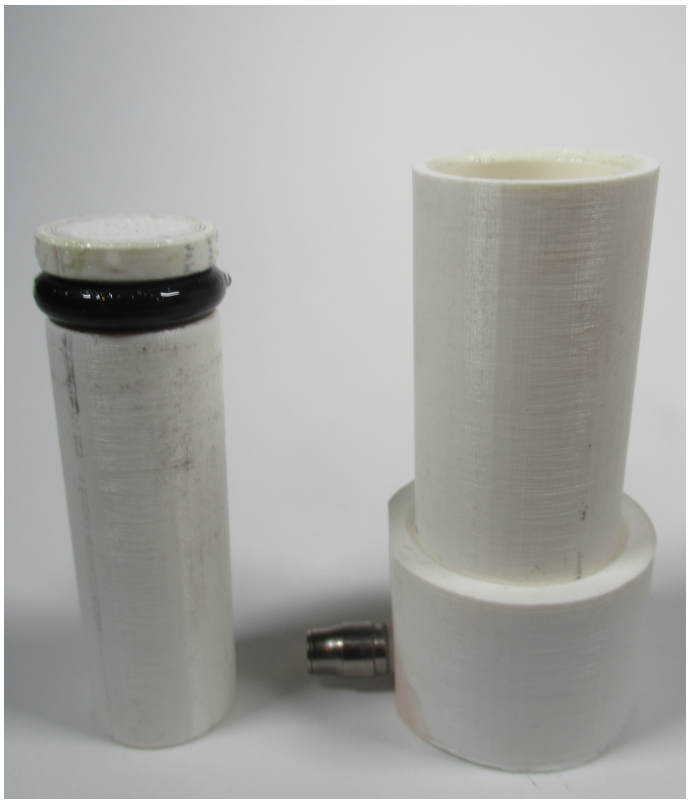

Figure 16: FDM printed PLA hydraulic piston (with O-ring) and cylinder.

3.1.2 SLA in Resin

Figure 17 presents the obtained SLA printed hydraulic piston-cylinder system.

Figure 17: SLA printed resin hydraulic piston-cylinder system.

3.1.3 SLM in Titanium

Figure 18 presents the obtained SLM printed hydraulic piston-cylinder system.

Figure 18: SLM printed Titanium hydraulic piston-cylinder system.

3.1.4 Machining Aluminium

Figure 19 presents the obtained machined hydraulic piston-cylinder system.

Figure 19: Machined Aluminum hydraulic piston-cylinder system.

3.2 Evaluation of the design

For each test set-up the results are shown below. However, no tests are shown about the SLM printed piston-cylinder system. The issue was that the water could flow through the material itself. A FDM printed piston was used with the SLM cylinder, and the water could flow through the cylinder, with drops appearing on its outer surface, even also small jets. Therefore, there was no option of increasing the pressure on the system´s fluid, making it impossible to perform any of the tests.

3.2.1 Static test

Following the steps mentioned on the static test protocol, in every trial the maximum of the sensor was reached, meaning that all the cylinders could withstand pressures up to 4 MPa without leakage or breakdown. The output of the tests is shown in Figures 20, 21, 22, 23 and 24.

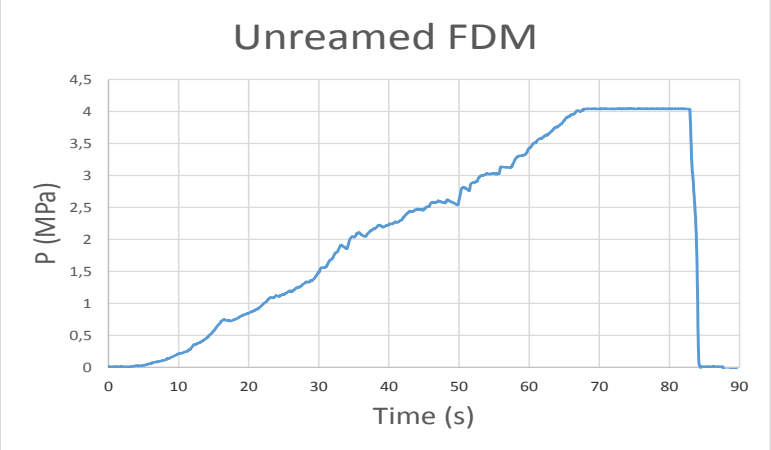

Figure 20: Static test´s measured pressure vs time for the unreamed FDM printed piston-cylinder system.

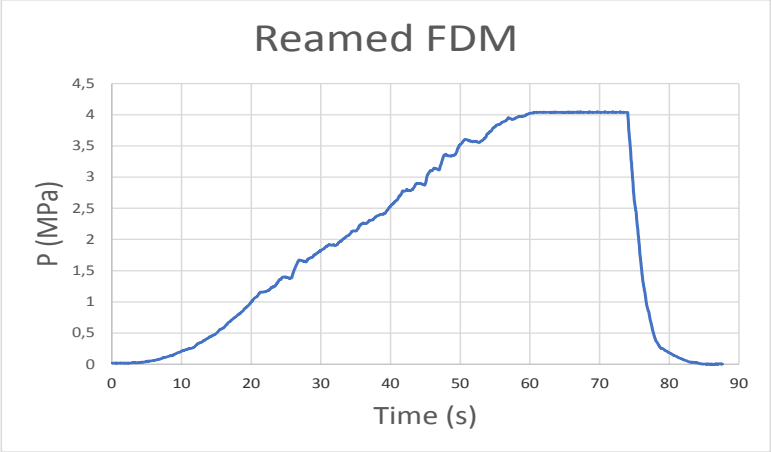

Figure 21: Static test´s measured pressure vs time for the reamed FDM printed piston-cylinder system.

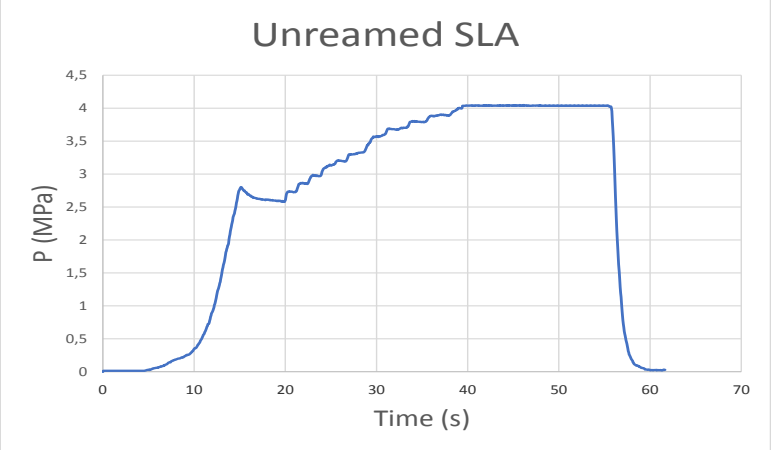

Figure 22: Static test´s measured pressure vs time for the unreamed SLA printed piston-cylinder system.

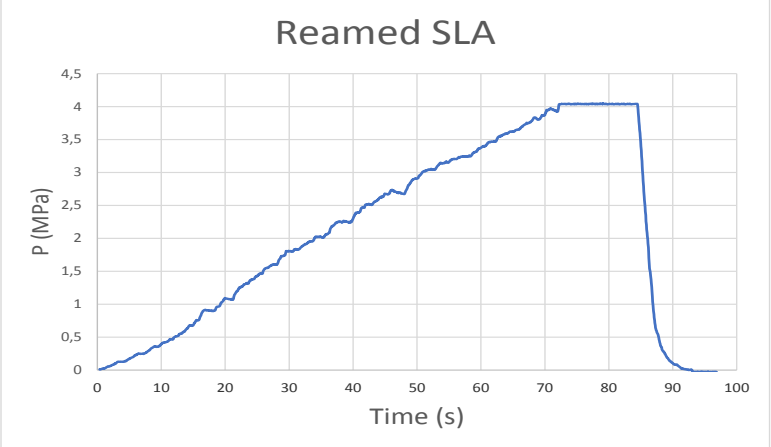

Figure 23: Static test´s measured pressure vs time for the reamed SLA printed piston-cylinder system.

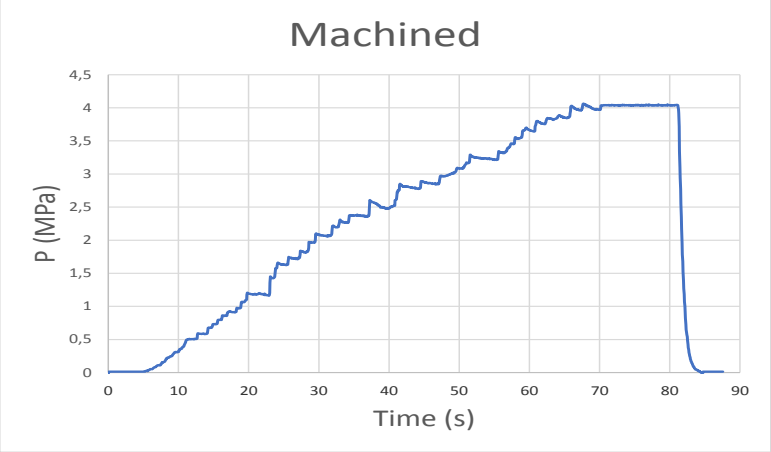

Figure 24: Static test´s measured pressure vs time for the machined piston-cylinder system.

3.2.2 Dynamic test

The protocol for the dynamic test was also followed to obtain the graphs of the pressure on the system´s fluid for each weight. Figures 25, 26, 27, 28 and 29 show the outcome of the tests.

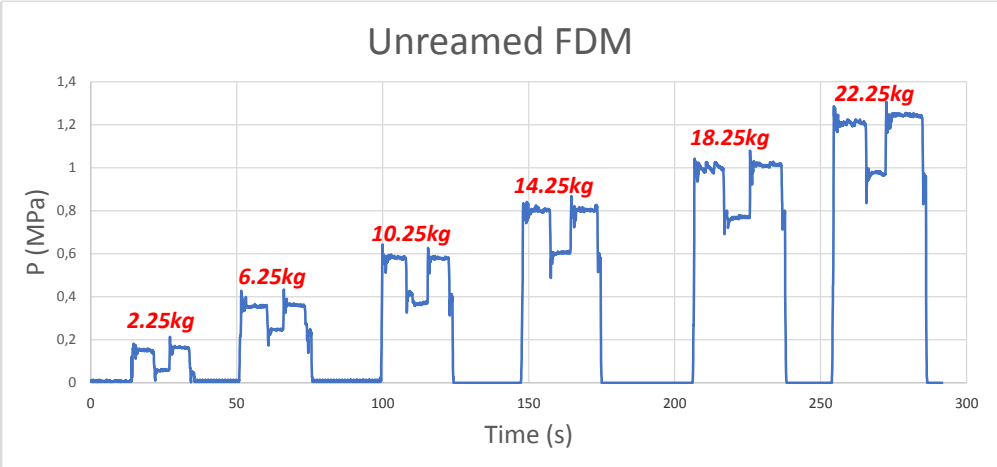

Figure 25: Dynamic test´s measured pressure vs time for the unreamed FDM printed piston-cylinder system. The weight (kg) lifted by the piston is indicated in red for each of the actuation cycles.

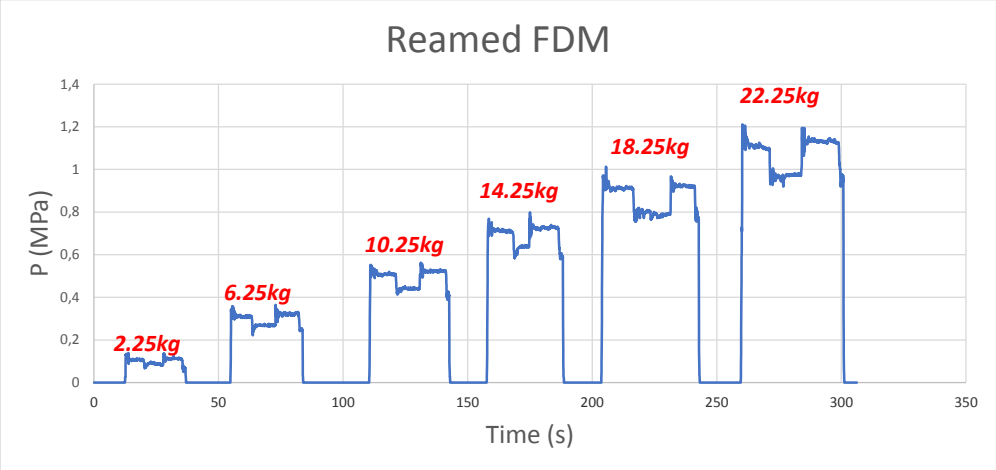

Figure 26: Dynamic test´s measured pressure vs time for the reamed FDM printed piston-cylinder system. The weight (kg) lifted by the piston is indicated in red for each of the actuation cycles.

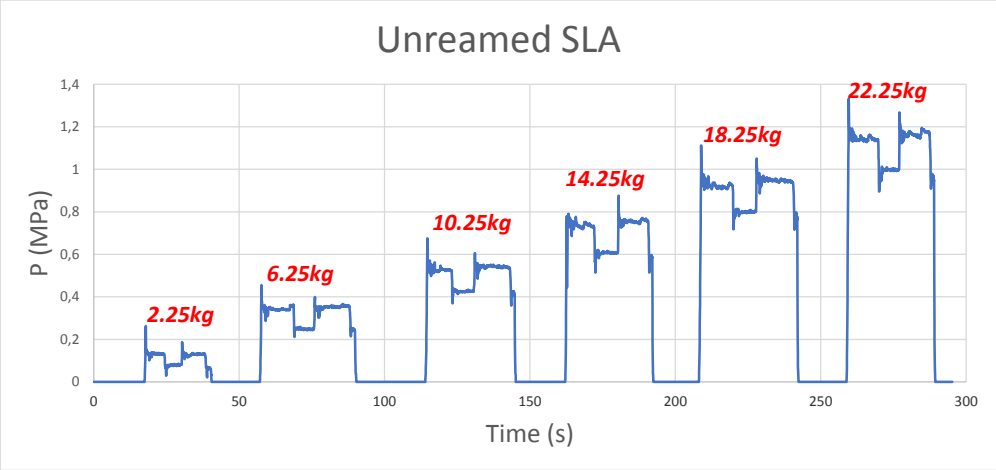

Figure 27: Dynamic test´s measured pressure vs time for the unreamed SLA printed piston-cylinder system. The weight (kg) lifted by the piston is indicated in red for each of the actuation cycles.

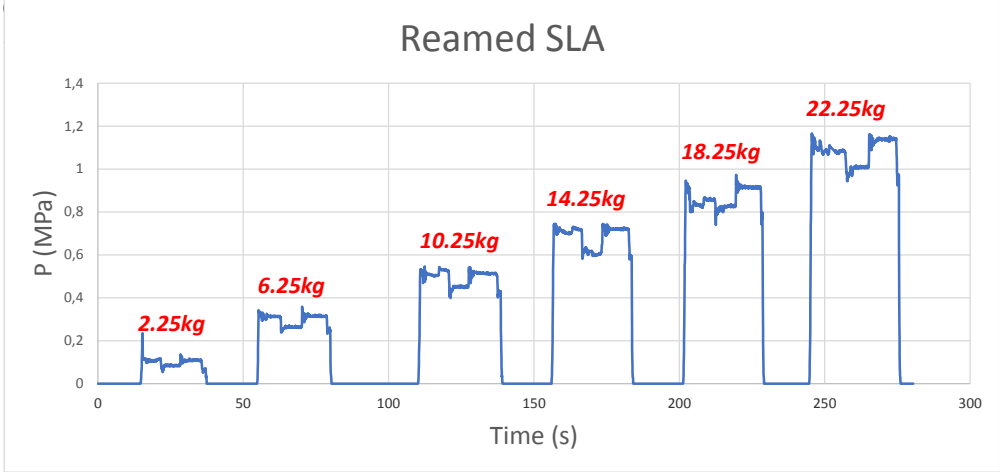

Figure 28: Dynamic test´s measured pressure vs time for the reamed SLA printed piston-cylinder system. The weight (kg) lifted by the piston is indicated in red for each of the actuation cycles.

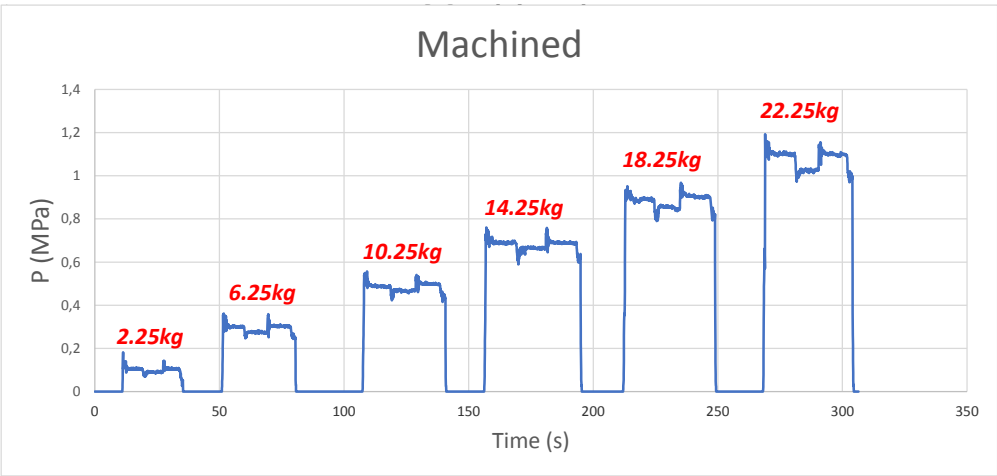

Figure 29: Dynamic test´s measured pressure vs time for the machined piston-cylinder system. The weight (kg) lifted by the piston is indicated in red for each of the actuation cycles.

It can be seen that for each weight, mainly two pressure values were measured, while theoretically one value can be calculated, as explained below:

It is known that

$$F = m * a = P * A \tag{12}$$

where,

F	Force actuating on the piston (N)
m	Mass (kg)
a	Acceleration (m/s^2)
P	Theoretical pressure of the system´s fluid (Pa)
A	Area of the piston where the fluid is acting (m^2)

$$A = \pi * D^2/4 \tag{13}$$

$$A = \pi * 0.016^2/4 = 2.01 * 10^{-4}\ m^2 \tag{14}$$

Solving for P from equation (12), and knowing that the only acceleration involved is gravity,

$$P = m * a/A = m * g/A \tag{15}$$

$$P = m * 9.81/2.01 * 10^{-4} = 48805.87 * m(Pa) \tag{16}$$

where,

g Gravitational acceleration (m/s^2)

The expression in equation (16) expresses the theoretical pressure (Pa) depending on the mass (kg) to be lifted. Table II includes the calculated theoretical pressures (MPa) for each of the weights.

Knowing that the shown calculations should be the theoretical pressures for each weight in the system, the obtained two different values for each weight are because of the friction, which always opposes to the movement [34]. Firstly, when the weights are lifted, the friction forces are on the same direction as the gravity, downwards. Therefore, more pressure is generated on the fluid to sustain the same weight. Secondly, when going down partially, the friction forces are pointing upwards, opposing gravity, meaning that a smaller pressure is enough to sustain the weight. As a consequence, the mean value between the two obtained pressures should ideally be equal to the theoretically calculated pressure. Table II compares the measured mean pressures for each weight and each production method with the calculated theoretical values.

Table II: Average measured and theoretically calculated pressures (in MPa) for each weight (in kg) and production method.

Production method	**Weights (kg)**					
	2.25	6.25	10.25	14.25	18.25	22.25
FDM	0.11	0.30	0.48	0.70	0.89	1.11
Reamed FDM	0.10	0.29	0.48	0.68	0.85	1.05
SLA	0.10	0.30	0.48	0.68	0.87	1.08
Reamed SLA	0.10	0.30	0.48	0.66	0.85	1.06
Machined	0.10	0.29	0.48	0.68	0.88	1.06
Theory	**0.11**	**0.30**	**0.50**	**0.70**	**0.89**	**1.09**

Secondly, it is possible to calculate the value of the frictional forces for each cylinder and each weight, as explained below with the example of the unreamed SLA cylinder, with a weight of 18.25 kg, as shown in Figure 30:

Figure 30: Measured pressure vs time on dynamic test of the unreamed SLA cylinder with 18.25 kg. The green arrows indicate the three plateaus, whereas the dotted line represents the average of the top and bottom plateaus.

$$\Delta P = Pplats - Pave \tag{17}$$

$$\Delta P = 0.933 - 0.866 = 0.067\ MPa \tag{18}$$

where,

$Pplats$	Average measured Pressure of the top plateaus of each weight (MPa)
$Pave$	Average measured Pressure between the top and bottom plateaus of each weight (MPa)
ΔP	Pressure difference between the plateaus and the average due to the friction (MPa)

As each plateau was around 8 seconds long, the average value of each plateau was calculated by using the points in the middle 5 seconds for the average. Converting the pressure difference ΔP into a force, the frictional force $Ffric$ was obtained:

$$Ffric = \Delta P * A \tag{19}$$

$$Ffric = 0.067 * 10^6 * 2.01 * 10^{-4} = 13.45\ N \tag{20}$$

Following the explained procedure for each case, the values in Figure 31 are obtained.

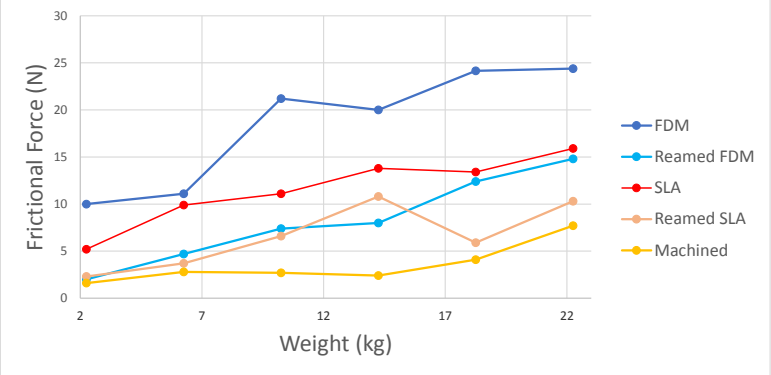

Figure 31: Friction forces for each weight and each production method.

Thirdly, as a final outcome of the dynamic test, the stick-slip friction for each case can also be deducted. The stick-slip phenomenon, which happens between two objects that are sliding over each other [35], in hydraulic cylinders it is characterized by a distinct stop-start movement of the cylinder. The static friction coefficient between two surfaces is larger than the kinetic friction coefficient, which implies a higher pressure build-up on the system to overcome the larger friction. This phenomenon was reflected on the dynamic test, every time that the relative movement between the piston and the cylinder was stopped and started again. Below it is explained how it was calculated, out of the graph from Figure 32 with the example of the unreamed SLA cylinder with a weight of 18.25 kg again:

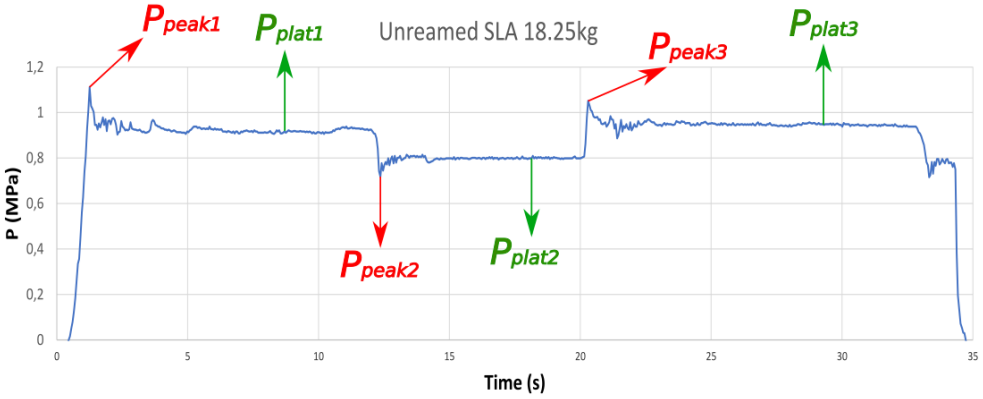

Figure 32: Measured pressure vs time on dynamic test of the unreamed SLA cylinder with 18.25 kg. The red arrows indicate the three peaks, whereas the green arrows indicate the three plateaus.

The pressure build-up because of the stick-slip phenomenon was reflected in a small peak of pressure achieved before reaching each plateau. Firstly, the difference of pressure between the peak and the plateau was calculated:

$$\Delta P_{stick1} = |P_{peak1} - P_{plat1}| \tag{21}$$

$$\Delta P_{stick1} = 1.12 - 0.92 = 0.2\ MPa \tag{22}$$

where,

P_{plat}	Average measured Pressure of each plateau (MPa)
P_{peak}	The local maximum/minimum pressure measured in each peak (MPa)
ΔP_{stick}	Pressure difference between each plateau and its peak due to the stick-slip (MPa)

For each weight, by making the average of the three pressure differences between each peak and each plateau, the mean pressure difference ΔP_{av} was obtained.

$$\Delta P_{av} = (\Delta P_1 + \Delta P_2 + \Delta P_3)/3 \tag{23}$$

$$\Delta P_{av} = (0.2 + 0.08 + 0.09)/3 = 0.12\ MPa \tag{24}$$

Converting the mean pressure difference ΔP_{av} into a force, the frictional force due to stick-slip $Fstick$ was obtained:

$$Fstick = \Delta P_{av} * A \tag{25}$$

$$Fstick = 0.12 * 10^6 * 2.01 * 10^{-4} = 24.1\ N \tag{26}$$

Following the explained procedure for each case, the values in Figure 33 were obtained.

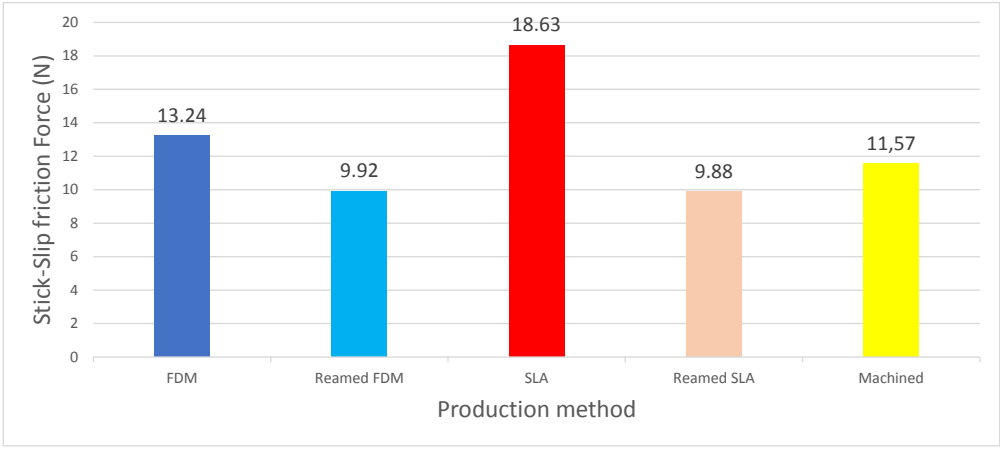

Figure 33: Stick-Slip friction forces for each production method.

4 Discussion

In this section the obtained results are discussed, while comparing the outcome of the carried out tests to point out the best performing options.

4.1 Design parameters

The mass of the piston-cylinder system is a relevant parameter for different applications where the weight can be critical. For example, prosthetic devices´main rejection reason is the weight [36]. Table I shows that there´s a considerable difference between the polymers and the metals, being the weight of the Ti and Al cylinders at least twice larger than the PLA and resin actuators. Between the metal cylinders, even if the density of Ti (4,5 g/cm^3) is much higher than the one of Al (2,7 g/cm^3), the weights are not that different, because the Al is a fully dense block while the infill of the Ti is smaller than 100%. On the other hand, the PLA and resin have similar densities (1.25 g/cm^3 and 1.2 g/cm^3, respectively) leading to similar weights as well.

Besides, the weight is useful to obtain the force-to-weight ratio. This indicator shows the weight needed by the actuator to provide with a desired mechanical force, which helps compare different kind of actuators between them [37]. It is calculated dividing the maximum force that the actuator can exert by the weight of it, both in the same units, usually in Newtons. The maximum achieved force was during the static test, reaching 4 MPa in all of them, which multiplied by the area of the piston, leads to a force of 804.4 N. The weight of the actuator is calculated by multiplying its mass in kg times the gravitational acceleration (g). Table III shows the force-to-weight ratio for each of the cylinders.

Table III: Maximum force (N), weight (N) and force-to-weight ratio (-) of each production method (the Max. Force of the SLM actuator is shown to compare it with the rest of the cylinders, even if it was not reached on the experiments).

Production	Max. Force (N)	Weight (N)	Force-To-Weight ratio (-).
FDM	804.4	0.023·g	3565
SLA	804.4	0.028·g	2928
SLM	804.4	0.064·g	1281
Machined	804.4	0.056·g	1464

As all of them achieved the same maximum force, the force-to-weight ratio only depends on the weight of each cylinder. Therefore, the polymeric actuators are able to achieve higher forces per kilogram of own weight.

The failure of the SLM printed Ti piston-cylinder system was because of the porosity of the printed parts. This is due to the way that the SLM parts are printed, one layer of powder on top of the next one, leading to a structure that is not waterproof. Also, because of the strength of the material, it is harder to apply post-processing tools to improve the surface quality, such as the reamer.

Moreover, it was desirable to test reaming on the cylinders, but this involved further post-processing steps that provoked the loss of one of the main benefits of 3D printing, the option of making a complex geometry in one single step. Still, it has shown to provoke smaller friction on the dynamic test (up to 40% less on the SLA, as can be deducted from the values from Figure 31) and less stick-slip friction (more than 45% difference on the SLA again, deducted from Figure 33 this time).

4.2 Evaluation parameters

As mentioned earlier, the static and dynamic tests led to results that allowed the comparison of each production method and material, as well as the reamed versions.

4.2.1 Static test parameters

The output of the performed static test is the maximum hydraulic pressure that the piston-cylinder system can handle with the used test set-up. It was demonstrated that the maximum pressure of the used sensor, 4 MPa, could be reached for all the studied piston-cylinder systems, without leakage or breakdown. Therefore, 3D printed hydraulic piston-cylinders could be applied in cases where the maximum pressure is below at least 4 MPa. The capability of an actuator of withstanding high pressures leads to the option of exerting high forces, which is a desirable capacity for applications where high forces are required.

4.2.2 Dynamic test parameters

The objective of the dynamic test was to replicate in a more realistic way the dynamic functioning of a piston-cylinder system, while being able to calculate the friction of each actuator via the measured pressure of the system´s fluid. At the same time, the calculated theoretical values could be compared to the measured results. Finally, the stick-slip friction could be obtained.

Table II compares the calculated theoretical pressures with the obtained average pressures for each cylinder with each weight. It can be deducted that the experiments correlate closely with the theory, but usually with slightly lower values on the tests. The maximum deviation in percentage is of 9 % in the case of the 2.25 kg, with an average measured pressure of 0.10 MPa in most of the cylinders, while the calculated pressure was 0.11 MPa. The reason for this can be the human influence, since the press handle had to be maintained manually at the same angle to keep the pressure constant. Another factor causing the small deviation could be a small calibration error of the sensor.

Figure 31 shows how the cylinder with lowest friction forces is the machined Al cylinder. This was expectable since the surface quality achievable by machining metals could not be reached by reaming polymers. Also, from the same Figure 31 it can be confirmed that reaming improves the surface quality, decreasing the frictional force. Finally, even if the reamer is used or not, in both cases the SLA cylinders have less friction that the FDM cylinders, as it was expected because of the printing quality. Therefore, the 3D printed version with the least friction was the reamed SLA actuator, with an average friction force of 6.6 N.

The last result of the dynamic test was the stick-slip friction of each cylinder. In this case the machined part is not the one with least friction, having the reamed cylinders the lowest stick-slip, both with a similar value of around 9.9 N of stick-slip frictional force, as shown in Figure 33. Unlike the dynamic friction, the stick-slip friction is higher on the unreamed SLA than on the unreamed FDM.

4.3 Comparison of results with the state-of-the-art

Table IV presents the maximum pressure achieved and the force-to-weight ratio of 3D printed fluidic (pneumatic and hydraulic) actuators developed during the last years. It shows that a maximum pressure of 1 MPa is reached (which is a 17% of the pressure achieved on this study) in the case of the only found 3D printed piston-cylinder system [2]. Table IV also demonstrates that this study presents the 3D printed fluidic actuator with the highest mentioned force-to-weight ratio of 3565, followed by a value of 26 (which is less than a 1% of the value from this study) in the case of a vacuum actuator lifting 26 times its own weight [38]. In comparison with the only found 3D printed

piston-cylinder system [2], there is also a big difference. The mentioned pneumatic cylinder has a weight of 0.33 kg (more than 10 times the weight of the polymer actuators from this study) with a maximum mentioned force of 45 N (which is a 6% of the achieved force in this study), leading to a force-to-weight ratio of 13.9.

Table IV: Maximum pressure (in MPa) and force-to-weight ratio (-) of 3D printed fluidic actuators.

Reference	Max. Pressure (MPa)	Force-to-weight ratio (-)
[39]	0.01	-
[40]	0.02	-
[41]	0.03	10
[42]	0.05	6
[43]	0.06	-
[38]	0.07	26
[41]	0.1	-
[44]	0.12	-
[45]	0.15	-
[46]	0.2	-
[47]	0.76	-
[48]	-	-
[2]	1	13.9
This study	4	3565

It should be considered that most of them are soft actuators, which could make it harder to achieve high pressures and forces, but also leads to lighter parts.

4.4 Limitations

The main limitation of the conducted research was the maximum pressure of 4 MPa measurable by the utilized sensor. With a sensor capable of measuring higher pressures, it would have been possible to reach the limit of each cylinder. Another constraint faced was the option of changing printing parameters, as well as the material for each 3D printing method. As the availability of the printers was limited and the prints could not be started by the author of this article, there was no opportunity to test several materials for each method and limited chance of testing different printing settings.

4.5 Future directions

The proposed cylinders demonstrated the ability of 3D printed hydraulic piston-cylinder actuators to withstand high pressures without leakage. Future developments of these cylinders should focus on the testing with higher pressures to reach the limit of each of them. In this way, the possible applications of the actuators could be broadened. A durability test would also be necessary to know the lifetime of the cylinders. Another option to increase the possibilities of applying the analyzed actuators in the real world would be changing the dimensions of it, to check that cylinders with smaller and larger diameter still perform adequately. Also, the End Cap and the cylinder were printed in two different parts to allow reaming of the whole inner surface of the cylinder in an easier way. However, if the reamer will not be used, both parts could be directly printed in one single piece, to avoid post-processing steps such as gluing. To overcome the encountered issue with the SLM printed parts, more prints with different printing settings could be tested, as well as trying the

Hot Isostatic Pressing to reduce its porosity and increase its density [49]. Finally, the 3D printed piston-cylinder systems should be tested in real applications as a next step after the used test set-ups, to verify that the actuators perform as desired in the aimed applications.

5 Conclusion

This study presents the design and validation of a 3D printed hydraulic piston-cylinder system, checking that it is feasible to produce them via additive manufacturing, in contrast with the conventional production methods. The same design was utilized for 3 different 3D printing methods, FDM, SLA and SLM, as well as for a machined version. Each of the samples was made of a different material, and all of them could reach more than 4 MPa without leakage or breakdown.

A second identical design was also created for each 3D printed cylinder to apply reaming, so that its performance could be compared with the unreamed versions. A dynamic test was performed to evaluate the performance of each piston-cylinder system. The measured experimental data followed closely the calculated theoretical values (the deviation was always below 9%). With the same test, the friction could also be calculated. The results showed that the best performing 3D printed option was the reamed SLA resin version, reaching pressures of at least 4 MPa, with a dynamic friction force of 6.6 N, a stick-slip friction force of 9.9 N and a weight of 28 g leading to a force-to-weight ratio of 2928. Only the machined Al version achieved a smaller dynamic friction, but with more than twice the weight.

The key finding of the conducted research is that the presented results mean a first step towards the 3D printing of hydraulic piston-cylinder systems: even if the friction is higher compared to a machined version, much lighter parts can be achieved that can benefit from the advantages of 3D printing while withstanding pressures higher than 4 MPa without leakage. Customizing and design freedom could be easier via FDM and SLA, enabling weight and geometry improvements in applications such as prosthesis.

References

[1] Jeffrey Plott and Albert Shih. The extrusion-based additive manufacturing of moisture-cured silicone elastomer with minimal void for pneumatic actuators. *Additive Manufacturing*, 17:1–14, oct 2017.

[2] Jeremy Krause, Pranav Bhounsule, Jeremy Krause, and Pranav Bhounsule. A 3D Printed Linear Pneumatic Actuator for Position, Force and Impedance Control. *Actuators*, 7(2):24, may 2018.

[3] Federico Montagnani, Gerwin Smit, Marco Controzzi, Christian Cipriani, and Dick H. Plettenburg. A passive wrist with switchable stiffness for a body-powered hydraulically actuated hand prosthesis. In *2017 International Conference on Rehabilitation Robotics (ICORR)*, pages 1197–1202. IEEE, jul 2017.

[4] ERIKS O-ring NBR 70 Compound 36624 — ERIKS shop NL, 15 July 2019.

[5] Barry Berman. 3-D printing: The new industrial revolution. *Business Horizons*, 55(2):155–162, mar 2012.

[6] Mari Koike, Preston Greer, Kelly Owen, Guo Lilly, Lawrence E. Murr, Sara M. Gaytan, Edwin Martinez, and Toru Okabe. Evaluation of Titanium Alloys Fabricated Using Rapid Prototyping Technologies—Electron Beam Melting and Laser Beam Melting. *Materials*, 4(10):1776–1792, oct 2011.

[7] C Lee Ventola. Medical Applications for 3D Printing: Current and Projected Uses. *P & T : a peer-reviewed journal for formulary management*, 39(10):704–11, oct 2014.

[8] Aslan Miriyev, Kenneth Stack, and Hod Lipson. Soft material for soft actuators. *Nature Communications*, 8(1):596, dec 2017.

[9] Juan Sebastian Cuellar, Gerwin Smit, Dick Plettenburg, and Amir Zadpoor. Additive manufacturing of non-assembly mechanisms. *Additive Manufacturing*, 21:150–158, may 2018.

[10] Ailish O'Halloran, Fergal O'Malley, and Peter McHugh. A review on dielectric elastomer actuators, technology, applications, and challenges. *Journal of Applied Physics*, 104(7):071101, oct 2008.

[11] Constantinos Mavroidis, Charles Pfeiffer, and Michael Mosley. 5.1 CONVENTIONAL ACTUATORS, SHAPE MEMORY ALLOYS, AND ELECTRORHEOLOGICAL FLUIDS. Technical report.

[12] M P M Dicker, J M Rossiter, I P Bond, and P M Weaver. Biomimetic photo-actuation: sensing, control and actuation in sun-tracking plants. *Bioinspiration & Biomimetics*, 9(3):036015, jun 2014.

[13] Victor Giurgiutiu. Review of Smart-Materials Actuation Solutions for Aeroelastic and Vibration Control. *Journal of Intelligent Material Systems and Structures*, 11(7):525–544, jul 2000.

[14] Sangbae Kim, Cecilia Laschi, and Barry Trimmer. Soft robotics: a bioinspired evolution in robotics. *Trends in Biotechnology*, 31(5):287–294, may 2013.

[15] Leonardo Ricotti, Barry Trimmer, Adam W. Feinberg, Ritu Raman, Kevin K. Parker, Rashid Bashir, Metin Sitti, Sylvain Martel, Paolo Dario, and Arianna Menciassi. Biohybrid actuators for robotics: A review of devices actuated by living cells. *Science Robotics*, 2(12):eaaq0495, nov 2017.

[16] Tuan D. Ngo, Alireza Kashani, Gabriele Imbalzano, Kate T.Q. Nguyen, and David Hui. Additive manufacturing (3D printing): A review of materials, methods, applications and challenges. *Composites Part B: Engineering*, 143:172–196, jun 2018.

[17] Ali Zolfagharian, Abbas Z. Kouzani, Sui Yang Khoo, Amir Ali Amiri Moghadam, Ian Gibson, and Akif Kaynak. Evolution of 3D printed soft actuators. *Sensors and Actuators A: Physical*, 250:258–272, oct 2016.

[18] Wen-Hong Zhu, E. Dupuis, and J.-C. Piedboeuf. Adaptive output force tracking control of hydraulic cylinders. In *Proceedings of the 2004 American Control Conference*, pages 5066–5071. IEEE, 2004.

[19] Gerwin Smit, Dick Plettenburg, and Frans Van der Helm. The Lightweight Delft Cylinder Hand, the First Multi-Articulating Hand That Meets the Basic User Requirements. *IEEE Transactions on Neural Systems and Rehabilitation Engineering*, pages 1–1, 2014.

[20] Michaël De Volder and Dominiek Reynaerts. Pneumatic and hydraulic microactuators: a review. *Journal of Micromechanics and Microengineering*, 20(4):043001, apr 2010.

[21] Leonard J. Martini. *Practical seal design*. M. Dekker, 1984.

[22] Parker Hannifin Corporation and Eps Division. Fluid Power Seal Design Guide, Catalog EPS 5370. Technical report, 2014.

[23] Eriks - Sealing Elements. ERIKS - Sealing Elements - Technical Handbook O-rings -. Technical report.

[24] John Ryan C. Dizon, Alejandro H. Espera, Qiyi Chen, and Rigoberto C. Advincula. Mechanical characterization of 3D-printed polymers. *Additive Manufacturing*, 20:44–67, mar 2018.

[25] L.-T. Lim, R. Auras, and M. Rubino. Processing technologies for poly(lactic acid). *Progress in Polymer Science*, 33(8):820–852, aug 2008.

[26] Ferry P.W. Melchels, Jan Feijen, and Dirk W. Grijpma. A review on stereolithography and its applications in biomedical engineering. *Biomaterials*, 31(24):6121–6130, aug 2010.

[27] Engineering Fit: Optimizing Design for Functional 3D Printed Assemblies. Technical report, 2017.

[28] Orienting a model, Formlabs Official Support, 23 July 2019.

[29] E.O. Olakanmi, R.F. Cochrane, and K.W. Dalgarno. A review on selective laser sintering/melting (SLS/SLM) of aluminium alloy powders: Processing, microstructure, and properties. *Progress in Materials Science*, 74:401–477, oct 2015.

[30] Donald M. Brunette, Pentti. Tengvall, Marcus. Textor, and Peter. Thomsen. *Titanium in Medicine : Material Science, Surface Science, Engineering, Biological Responses and Medical Applications*. Springer Berlin Heidelberg, 2001.

[31] Dimensional accuracy of 3D printed parts — 3D Hubs.

[32] Mário C Santos, Alisson R Machado, Wisley F Sales, Marcos A S Barrozo, and Emmanuel O Ezugwu. Machining of aluminum alloys: a review.

[33] Roshani U Shingarwade and Pankaj S Chavan. A REVIEW ON MQL IN REAMING. Technical report, 2014.

[34] S. Jack Burrow. Friction and resistance to sliding in orthodontics: A critical review. *American Journal of Orthodontics and Dentofacial Orthopedics*, 135(4):442–447, apr 2009.

[35] Alan D Berman, William A Ducker, and Jacob N Israelachvili. Origin and Characterization of Different Stick-Slip Friction Mechanisms †. Technical report, 1996.

[36] Elaine Biddiss, Dorcas Beaton, and Tom Chau. Consumer design priorities for upper limb prosthetics. *Disability and rehabilitation. Assistive technology*, 2(6):346–57, nov 2007.

[37] A Della Santa, D De Rossi, and A Mazzoldi. Performance and work capacity of a polypyrrole conducting polymer linear actuator. Technical report, 1997.

[38] Charbel Tawk, Marc in het Panhuis, Geoffrey M. Spinks, and Gursel Alici. Bioinspired 3D Printable Soft Vacuum Actuators for Locomotion Robots, Grippers and Artificial Muscles. *Soft Robotics*, 5(6):685–694, dec 2018.

[39] Alfonso Costas, Daniel E. Davis, Yixian Niu, Sadegh Dabiri, Jose Garcia, and Brittany Newell. Design, Development and Characterization of Linear, Soft Actuators via Additive Manufacturing. In *Volume 1: Development and Characterization of Multifunctional Materials; Modeling, Simulation, and Control of Adaptive Systems; Integrated System Design and Implementation*, page V001T01A018. ASME, sep 2018.

[40] Lisen Ge, Longteng Dong, Dong Wang, Qi Ge, and Guoying Gu. A digital light processing 3D printer for fast and high-precision fabrication of soft pneumatic actuators. *Sensors and Actuators A: Physical*, 273:285–292, apr 2018.

[41] Kunhao Yu, An Xin, Haixu Du, Ying Li, and Qiming Wang. Additive manufacturing of self-healing elastomers.

[42] John Morrow, Samantha Hemleben, and Yigit Menguc. Directly Fabricating Soft Robotic Actuators With an Open-Source 3-D Printer. *IEEE Robotics and Automation Letters*, 2(1):277–281, jan 2017.

[43] Martin Manns, Jorge Morales, and Peter Frohn. Additive manufacturing of silicon based PneuNets as soft robotic actuators. *Procedia CIRP*, 72:328–333, jan 2018.

[44] Authors Byrne, James F X, and Ní Annaidh. Title Additive Manufacture of Composite Soft Pneumatic Actuators. 2018.

[45] Ryan L. Truby, Michael Wehner, Abigail K. Grosskopf, Daniel M. Vogt, Sebastien G. M. Uzel, Robert J. Wood, and Jennifer A. Lewis. Soft Somatosensitive Actuators via Embedded 3D Printing. *Advanced Materials*, 30(15):1706383, apr 2018.

[46] Hao Hsu, Liang-Yen Liu, Ling-Ying Liu, and Yu-Chuan Su. 3D manufactured, water-powered soft actuators for orthodontic application. *Smart Materials and Structures*, 27(8):084006, aug 2018.

[47] David B. Comber, Jonathon E. Slightam, Vito R. Gervasi, Joseph S. Neimat, and Eric J. Barth. Design, Additive Manufacture, and Control of a Pneumatic MR-Compatible Needle Driver. *IEEE Transactions on Robotics*, 32(1):138–149, feb 2016.

[48] Paul Guerrier and Christopher Bowen. Additive manufacturing for next generation actuation, 2016.

[49] Rimit Kumar, Ashok Kumar Jain, V A Popovich, S M Ahmadi, and J Zhou. Influence of post-processing on Ti6Al4V lattice structures produced by Selective Laser Melting. Technical report, 2017.

Appendix A: 3D printed materials' datasheets

- FDM: PLA

Ultimaker

Mechanical properties*

	Injection molding		3D printing	
	Typical value	**Test method**	**Typical value**	**Test method**
Tensile modulus	-	-	2,346.5 MPa	ISO 527 (1 mm/min)
Tensile stress at yield	-	-	49.5 MPa	ISO 527 (50 mm/min)
Tensile stress at break	-	-	45.6 MPa	ISO 527 (50 mm/min)
Elongation at yield	-	-	3.3%	ISO 527 (50 mm/min)
Elongation at break	-	-	5.2%	ISO 527 (50 mm/min)
Flexural strength	-	-	103 MPa	ISO 178
Flexural modulus	-	-	3,150 MPa	ISO 178
Izod impact strength, notched (at 23 °C)	-	-	5.1 kJ/m^2	ISO 180
Charpy impact strength (at 23 °C)	-	-	-	
Hardness	-	-	83 (Shore D)	Durometer

Electrical properties*

	Typical value	**Test method**	**Typical value**	**Test method**
Dissipation factor (at 1 MHz)	-	-	0.008	ASTM D150-11
Dielectric constant (at 1 MHz)	-	-	2.70	ASTM D150-11

Thermal properties

	Typical value	**Test method**
Melt mass-flow rate (MFR)	6.09 g/10 min	ISO 1133 (210 °C, 2.16 kg)
Heat detection (at 0.455 MPa)	-	-
Heat deflection (at 1.82 MPa)	-	-
Vicat softening temperature	-	-
Glass transition	~ 60 °C	ISO 11357
Coefficient of thermal expansion	-	-
Melting temperature	145 - 160 °C	ISO 11357
Thermal shrinkage	-	-

Filament specifications

	Value	**Method**
Diameter	2.85 ± 0.10 mm	-
Max roundness deviation	0.10 mm	-
Net filament weight	350 g / 750 g	-
Filament length	~ 44 m / ~ 95 m	-

Other properties

	Value	**Test method**
Specific gravity	1.24	ASTM D1505
Flame classification	-	-

- **SLA: Resin**

Material Properties Data

The following material properties are comparable for all Formlabs Standard Resins.

	METRIC[1]		IMPERIAL[1]		METHOD
	Green[2]	Post-Cured[3]	Green[2]	Post-Cured[3]	
Tensile Properties					
Ultimate Tensile Strength	38 MPa	65 MPa	5510 psi	9380 psi	ASTM D 638-10
Tensile Modulus	1.6 GPa	2.8 GPa	234 ksi	402 ksi	ASTM D 638-10
Elongation at Failure	12 %	6.2 %	12 %	6.2 %	ASTM D 638-10
Flexural Properties					
Flexural Modulus	1.25 GPa	2.2 GPa	181 ksi	320 ksi	ASTM C 790-10
Impact Properties					
Notched IZOD	16 J/m	25 J/m	0.3 ft-lbf/in	0.46 ft-lbf/in	ASTM D 256-10
Temperature Properties					
Heat Deflection Temp. @ 264 psi	42.7 °C	58.4 °C	108.9 °F	137.1 °F	ASTM D 648-07
Heat Deflection Temp. @ 66 psi	49.7 °C	73.1 °C	121.5 °F	163.6 °F	ASTM D 648-07

[1] Material properties can vary with part geometry, print orientation, print settings, and temperature.

[2] Data was obtained from green parts, printed using Form 2, 100 µm, Clear settings, washed and air dried without post cure.

[3] Data was obtained from parts printed using Form 2, 100 µm, Clear settings, and post-cured with 1.25 mW/cm^2 of 405 nm LED light for 60 minutes at 60 °C.

- **SLM: Titanium**

High purity titanium: Ti-6Al-4V Grade 23

Powder chemistry may comply with standards: ASTM B348, ASTM F136, ASTM F1580, ASTM F2924, ASTM F3001, AMS 4998
Typical particle size distributions (PSD): 0-20 µm, 15-45 µm, 15-63 µm, 45-106 µm, 45-150 µm, 106-180 µm

SD	Size distribution by laser diffraction (ASTM B822)			Apparent density (ASTM B212)	Flow rate (ASTM B213)	Oxygen content
	D10	D50	D90			
0-20 µm	6 µm	13 µm	19 µm	2.8 g/cm^3*	--	--
15-45 µm	20 µm	34 µm	44 µm	2.49 g/cm^3	28 s	0.11 %
15-63 µm	24 µm	44 µm	61 µm	2.50 g/cm^3	25 s	0.10 %
45-106 µm	52 µm	71 µm	102 µm	2.47 g/cm^3	24 s	0.08 %
45-150 µm	54 µm	81 µm	123 µm	2.59 g/cm^3	25 s	0.08 %

*Tap density per ASTM B527

Appendix B: 3D printers' datasheets

- FDM: Ultimaker 3

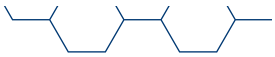

Ultimaker 3 specifications

Printer and printing properties	Technology	Fused filament fabrication (FFF)
	Print head	Dual extrusion print head with a unique auto-nozzle lifting system and swappable print cores
	Build volume (XYZ)	Single extrusion: 215 x 215 x 200 mm (8.5 x 8.5 x 7.9 in) Dual extrusion: 197 x 215 x 200 mm (7.8 x 8.5 x 7.9 in)
	Layer resolution	0.25 mm nozzle: 150 - 60 micron 0.4 mm nozzle: 200 - 20 micron 0.8 mm nozzle: 600 - 20 micron
	XYZ resolution	12.5, 12.5, 2.5 micron
	Build speed	< 24 mm^3/s
	Build plate	Heated glass build plate (20 - 100 °C)
	Nozzle diameter	0.4 mm (included) 0.25 mm, 0.8 mm (sold separately)
	Operating sound	< 50 dBA
	Connectivity	Wi-Fi, LAN, USB port
Physical dimensions	Dimensions (with Bowden tubes and spool holder)	342 x 505 x 588 mm (13.5 x 19.9 x 23.1 in)
	Net weight	10.6 kg (23.4 lbs)
Software	Supplied software	Ultimaker Cura, our free print preparation software Ultimaker Connect, our free printer management solution Ultimaker Cloud, enables remote printing
	Supported OS	Windows, MacOS, Linux
Warranty	Warranty period	12 months

- SLA: Formlabs 2

formlabs

Optical Path
Protected
Printer control
Interactive Touch-screen with Push-button

Hardware

Dimensions
35 × 33 × 52 cm
13.5 × 13 × 20.5 in
Weight
13 kg
28.5 lbs

Operating Temperature
Auto-heats to 35° C
Auto-heats to 95° F
Temperature Control
Self-heating Resin Tank

Power Requirements
100–240 V
1.5 A 50/60 Hz
65 W

Laser Specifications
EN 60825-1:2007 certified
Class 1 Laser Product
405nm violet laser
250mW laser

Connectivity
Wifi, Ethernet and USB

Printing Properties

Technology
Stereolithography (SLA)
Peel Mechanism
Sliding Peel Process with wiper
Resin Fill System
Automated

Build Volume
145 × 145 × 175 mm
5.7 × 5.7 × 6.9 in

Layer Thickness (Axis Resolution)
25, 50, 100 microns
0.001, 0.002, 0.004 inches
Laser Spot Size (FWHM)
140 microns
0.0055 inches

Supports
Auto-Generated
Easily Removable

Material Properties

Packaging
1 L cartridges

- **SLM: SLM 125**

Technical Specifications

Build Envelope (L x W x H)	125 x 125 x 125 mm reduced by substrate plate thickness
Build Volume Reduction	50 x 50 x 50 mm reduced by substrate plate thickness
3D Optics Configuration	Single (1x 400 W) IPG fiber laser
Build Rate	up to 25 cm^3/h
Variable Layer Thickness	20 µm - 75 µm, 1 µm increments
Min. Feature Size	140 µm
Beam Focus Diameter	70 µm - 100 µm
Max. Scan Speed	10 m/s
Average Inert Gas Consumption in Process	0,6 l/min (argon)
Average Inert Gas Consumption Purging	70 l/min (argon)
E-Connection / Power Input	400 Volt 3NPE, 32 A, 50/60 Hz, 3 kW
Compressed Air Requirement / Consumption	ISO 8573-1:2010 [1:4:1], 50 l/min @ 6 bar
Dimensions (L x W x H)	1400 mm x 900 mm x 2460 mm
Weight (without / incl. powder)	approx. 700 kg / approx. 750 kg

System configuration for all types of metal powders
Technical changes reserved